British Journal of Cancer www.nature.com/bjc

ARTICLE

Translational Therapeutics

Tumour microenvironment characterisation to stratify patients for hyperthermic intraperitoneal chemotherapy in high-grade serous ovarian cancer (OVHIPEC-1)

S. Lot Aronson[1,2,22], Cédric Walker[3,4,22], Bram Thijssen[5,6], Koen K. van de Vijver[1,7], Hugo M. Horlings[8], Joyce Sanders[8], Maartje Alkemade[9], Simone N. Koole[1], Marta Lopez-Yurda[10], Christianne A. R. Lok[1], OVHIPEC-1 Study Group*, Sven Rottenberg[3,11], Jacco van Rheenen[12], Gabe S. Sonke[2], Willemien J. van Driel[1]✉, Lennart A. Kester[13,23] and Kerstin Hahn[12,23]

BACKGROUND: Hyperthermic intraperitoneal chemotherapy (HIPEC) improves survival in patients with Stage III ovarian cancer following interval cytoreductive surgery (CRS). Optimising patient selection is essential to maximise treatment efficacy and avoid overtreatment. This study aimed to identify biomarkers that predict HIPEC benefit by analysing gene signatures and cellular composition of tumours from participants in the OVHIPEC-1 trial.
METHODS: Whole-transcriptome RNA sequencing data were retrieved from high-grade serous ovarian cancer (HGSOC) samples from 147 patients obtained during interval CRS. We performed differential gene expression analysis and applied deconvolution methods to estimate cell-type proportions in bulk mRNA data, validated by histological assessment. We tested the interaction between treatment and potential predictors on progression-free survival using Cox proportional hazards models.
RESULTS: While differential gene expression analysis did not yield any predictive biomarkers, the cellular composition, as characterised by deconvolution, indicated that the absence of macrophages and the presence of B cells in the tumour microenvironment are potential predictors of HIPEC benefit. The histological assessment confirmed the predictive value of macrophage absence.
CONCLUSION: Immune cell composition, in particular macrophages absence, may predict response to HIPEC in HGSOC and these hypothesis-generating findings warrant further investigation.
CLINICAL TRIAL REGISTRATION: NCT00426257.

British Journal of Cancer; https://doi.org/10.1038/s41416-024-02731-6

BACKGROUND

Hyperthermic intraperitoneal chemotherapy (HIPEC) improves survival in patients with Stage III ovarian cancer following neoadjuvant chemotherapy (NACT) and interval cytoreductive surgery (CRS) [1, 2]. Following the publication of the OVHIPEC-1 trial, this treatment modality has been included in several international guidelines as a treatment option [3–6]. The OVHIPEC-1 trial showed, at a median follow-up period of 10.1 years, that the addition of cisplatin-based HIPEC to CRS significantly improved progression-free survival (HR 0.66 [95% CI 0.50–0.87], stratified $P = 0.0031$) and overall survival (HR 0.67 [95% CI 0.48–0.94], stratified $P = 0.019$) when compared to surgery alone. These findings were confirmed in a Korean randomised controlled trial for the specific patient population treated with NACT and interval CRS, although no significant advantage of HIPEC was observed in the overall patient population, which included patients with Stage IV disease and those treated with primary CRS [7]. The differential response observed across patient subgroups highlights the importance of identifying biomarkers to effectively select patients for HIPEC in order to optimise treatment efficacy and avoid overtreatment.

[1]Center for Gynecologic Oncology Amsterdam, Department of Gynecologic Oncology, The Netherlands Cancer Institute, Amsterdam, The Netherlands. [2]Department of Medical Oncology, The Netherlands Cancer Institute, Amsterdam, The Netherlands. [3]Institute of Animal Pathology, Vetsuisse Faculty, University of Bern, Bern, Switzerland. [4]Graduate School for Cellular and Biomedical Sciences, University of Bern, Bern, Switzerland. [5]Division of Molecular Carcinogenesis, Oncode Institute, Netherlands Cancer Institute, Amsterdam, The Netherlands. [6]Oncode Institute, Utrecht, The Netherlands. [7]Department of Pathology & Cancer Research Institute Ghent (CRIG), Ghent University Hospital, Ghent, Belgium. [8]Department of Pathology, The Netherlands Cancer Institute, Amsterdam, The Netherlands. [9]Core Facility Molecular Pathology and Biobanking, The Netherlands Cancer Institute, Amsterdam, The Netherlands. [10]Department of Biometrics, The Netherlands Cancer Institute, Amsterdam, The Netherlands. [11]Bern Center for Precision Medicine, University of Bern, Bern, Switzerland. [12]Department of Molecular Pathology, Oncode Institute, The Netherlands Cancer Institute, Amsterdam, The Netherlands. [13]Princess Máxima Center for Pediatric Oncology, Utrecht, The Netherlands. [22]These authors contributed equally: S. Lot Aronson, Cédric Walker. [23]These authors jointly supervised this work: Lennart A. Kester, Kerstin Hahn. *A list of authors and their affiliations appears at the end of the paper. ✉email: w.v.driel@nki.nl

Received: 19 December 2023 Revised: 14 May 2024 Accepted: 17 May 2024
Published online: 12 June 2024

Alongside the malignant epithelial cells, non-malignant cell populations present in the tumour microenvironment (TME) are increasingly recognised to modulate tumour behaviour and therapeutic response [8–14]. Cell components in the TME can be classified into immune cells and stromal cells and include cancer-associated fibroblasts (CAF), endothelial cells, macrophages, dendritic cells, and lymphocytes. In this study, we aim to explore the TME as a source of predictive biomarkers for patient stratification in the context of HIPEC.

While conventional bulk transcriptome analysis provides valuable insights into the average gene expression profile of a tumour, the assessment of cellular heterogeneity within the tumour is limited. Single-cell RNA sequencing (RNA-seq) has emerged as a technique to overcome this constraint by allowing analysis of gene expression at the level of individual cells. However, its use is hampered by technical complexity, limited throughput, cost, and labour-intensiveness. Hence, deconvolution methods offer an alternative to obtain comparable insights into tumour heterogeneity [15–18].

Deconvolution is a computational technique to infer the proportions of different cell types in tissue samples from bulk mRNA-seq data, using reference profiles derived from single-cell sequencing for each cell type in the tumour [16, 17, 19, 20]. A notable advantage of this approach over traditional pathology lies in its ability to provide richer and more nuanced information about the cellular landscape, including distinctions between subpopulations of epithelial cells and other cells in the TME. While deconvolution of bulk RNA-seq has proven useful in breast cancer and other tumour types in predicting treatment and survival outcomes [18, 21–24], its accuracy and applicability to predict HIPEC response in HGSOC remains unexplored.

The objective of this study is twofold: first, to evaluate the cellular makeup of the tumour and surrounding TME in tissue samples from participants in the OVHIPEC-1 trial using deconvolution of bulk RNA-seq data; and second, to utilise this cellular profile alongside differential expression analysis of bulk mRNA-seq data and morphologic features to predict response to HIPEC.

METHODS

Trial design and participants

OVHIPEC-1 is a multicentre, open-label, randomised, controlled, Phase 3 trial conducted at eight experienced HIPEC centres in the Netherlands and Belgium between April 1, 2007 and April 30, 2016. The study design, eligibility criteria, and procedures have been described in detail previously [1]. In brief, a total of 245 patients with histologically confirmed primary Stage III epithelial ovarian, fallopian tube, or peritoneal cancer were enrolled and randomly assigned to undergo interval CRS either with or without HIPEC, stratified according to previous suboptimal CRS (yes vs. no), the institution performing the surgery, and the number of regions involved in the abdominal cavity (0–5 vs. 6–8).

Study oversight

OVHIPEC-1 was an investigator-initiated trial with Netherlands Cancer Institute being the sponsor. The local ethics board of all participating sites approved the study protocol. The study was conducted in accordance with the ICH Harmonised Tripartite Guideline for Good Clinical Practice and the principles of the Declaration of Helsinki. All patients provided written informed consent. This study is registered with ClinicalTrials.gov, NCT00426257.

Treatment

All patients were treated with at least three cycles of neoadjuvant carboplatin (area under the curve of 5–6 mg/ml/min) and paclitaxel (175 mg/m^2 of body-surface area) once every three weeks and were eligible for the study if they had not progressed during these cycles. The HIPEC procedure has been described in detail previously. In brief, heated saline (40–42 °C) was continuously circulated through the abdominal cavity for 90 minutes using the open technique. Cisplatin was added at a dose of 100 mg/m^2. Sodium thiosulfate was administered to prevent nephrotoxicity. Adjuvant chemotherapy consisted of three additional cycles of carboplatin (area under the curve of 5–6 mg/ml/min) and paclitaxel (175 mg/m^2 of body-surface area) once every three weeks for patients in both arms. Accrual in the OVHIPEC-1 trial was completed before the reimbursement of poly (ADP-ribose) polymerase inhibitors (PARPi) as frontline maintenance therapy. However, two patients participated in the SOLO-1 trial with olaparib versus placebo in this setting [25]. As per Dutch national guidelines, patients did not receive bevacizumab maintenance therapy following frontline treatment.

Endpoints and statistical considerations

The primary endpoint was progression-free survival (PFS), which was defined as the time from randomisation to disease recurrence, progression, or death from any cause, whichever occurred first. Disease progression was defined according to Response Evaluation Criteria in Solid Tumours version 1.1, or on the basis of an increased CA-125 level, whichever one of these two criteria was met first, as recommended by the Gynecologic Cancer InterGroup [26]. Overall survival (OS) was a secondary endpoint and was defined as the time from randomisation to death of any cause. Survival data were censored at the date of last contact for those patients who had no evidence of disease or remained alive, with a cut-off date of March 31, 2022 (median follow-up of 10.1 years).

Tissue was collected to study gene expression profiles in the tumour to identify subgroups of patients that differ in their benefit from HIPEC therapy, which is the objective of the current study.

For descriptive statistics, the (nonparametric) Wilcoxon's rank-sum test (Mann–Whitney *U* test) was employed for differences between numerical variables. Categorical variables were compared using Fisher's two-sided exact test. All reported *P* values were two-sided, and statistical significance was established when the *P* value was less than 0.05 in all cases.

Baseline and treatment characteristics of patients with available tissue samples for histopathologic evaluation (histopathology cohort) were balanced between treatment arms (Supplementary Table 2). In the cohort of patients with available RNA-seq data (RNA-seq cohort), there was a significant difference between treatment arms in the time between surgery and adjuvant chemotherapy (Supplement Table 3). Adjustment for this variable did not negatively impact the effect of HIPEC treatment (HR for PFS 0.72 [95% CI 0.56–1.09] and HR for OS 0.71 [95% CI 0.49–1.01]) and therefore the time between surgery and adjuvant chemotherapy did not confound the association between treatment and PFS. Characteristics of the current study cohorts were largely similar to those of the excluded patients. However, a notable difference was a higher prevalence of previous suboptimal surgery in the included patients (Supplementary Tables 4 and 5).

Hazard ratios and their corresponding 95% confidence intervals were estimated using (stratified) Cox proportional hazards (CPH) models. The assumption of proportional hazards was evaluated by both graphical inspection of scaled Schoenfeld residuals and a test for independence between residuals and time. In the case of non-proportionality, the corresponding variable was added as a stratification variable to the CPH model. Subgroup analyses were presented with first-order interaction *P* values ($\alpha = 0.05$), which were obtained using the likelihood-ratio test involving nested models containing and excluding the interaction term.

Tissue availability

Only patients with HGSOC were included for this study. Figures 1 and 2 provide a summary of tissue sample collection and RNA-seq data for the participants in the study, as well as a summary of the methods. Reasons for sample unavailability include withdrawal of consent, complete pathologic response after NACT (i.e., no detectable tumour remaining), insufficient RNA quality, or failure to receive samples from the participating sites.

Tissue samples

Formalin-fixed, paraffin-embedded (FFPE) tissue was collected at three time points: (1) pre-treatment; (2) surgical resection (during interval CRS before the administration of HIPEC); and (3) at disease recurrence. Tissue samples were obtained from either primary tumours or metastatic sites. Pre-treatment histology was not available for all patients, as the diagnosis was based on ascites cytology in the majority of patients.

Histopathological assessment

Histopathologic evaluation was performed by three experienced gynecologic pathologists (KKvdV, HMH, JS) on tissue resected during interval CRS with the online platform Slidescore (www.slidescore.com). The following variables

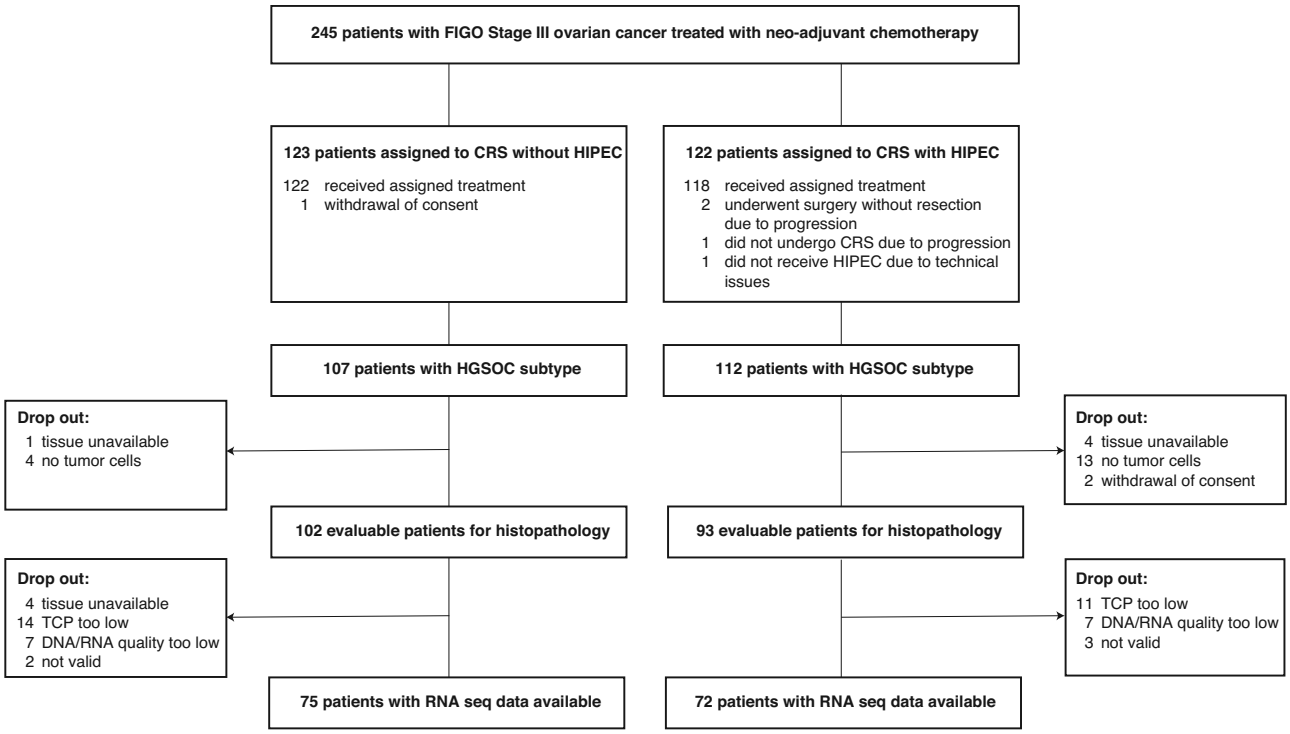

Fig. 1 CONSORT diagram of OVHIPEC-1 participants and tissue availability. HGSOC high-grade serous ovarian cancer, TCP tumour cell percentage, CRS cytoreductive surgery, HIPEC hyperthermic intraperitoneal chemotherapy.

were manually scored on routine haematoxylin and eosin (H&E)-stained sections: growth pattern (glandular, papillary, solid, or a combination, mitotic rate (< 12 or ≥12), psammoma bodies (present or absent), stromal and intra-epithelial TILs (as a percentage of the tumour area), tertiary lymphoid structures (present or absent), macrophages (present or absent), fibrosis (present or absent), necrosis (present or absent), and tumour regression score (based on Mandard score [27], classified from 1 to 5).

RNA isolation and sequencing

RNA was isolated from FFPE samples containing at least 30% tumour cells. A pathologist (JS) scored the tumour percentage and indicated the most tumour-dense region on an H&E-stained slide for subsequent RNA isolation. Five to 10 FFPE slides (10 µm) were used for isolation of RNA using the AllPrep DNA/RNA FFPE isolation kit (Qiagen, 80234) in combination with the QIAcube, following the manufacturer's recommended protocol. For sequencing, Truseq RNA Exome Prep method was used. The data generated were single-end reads with a length of 65 base pairs. Sequencing was performed on the HiSeq 2500 platform using High Output Mode with the HOM SR Cluster Kit v4 and chemistry v4.

Sequencing data were aligned to the hg38 reference genome using the Rsem package. The alignment and transcript quantification were executed using STAR with default parameters within the Rsem package [28, 29]. Transcripts per million values were further used in the deconvolution pipeline, while expected count values were used for differential expression analysis.

Bulk mRNA sequencing analysis

Differentially expression genes were identified using DESeq2 [30], using the expected counts from the STAR alignment described above. First, for two samples that were sequenced twice, the two duplicate sample read counts were added together. Next, we removed genes with less than 500 reads across all samples, and genes that did not have at least 10 samples with at least 20 reads, leaving 20,078 genes for differential expression analysis. For the remaining analysis, all standard settings of the DESeq2 R package were used.

For the association of genes with PFS, we first estimated the log-transformed counts per million using the variance stabilising transform, and using the sample location (primary tumour vs metastasis) as cofactor in estimating the variance. The effect of an interaction between the resulting transformed counts per million and treatment were tested against PFS in a CPH model. *P* values were adjusted for multiple testing with Benjamini–Hochberg correction.

For identifying differentially expressed genes, we compared several subgroups: (1) primary tumour samples versus metastatic samples and (2) pre-treatment samples versus resection samples, with location as cofactor. For differential gene set enrichment analysis, we used the flexgsea R package [31] with the default weighted KS-like statistic [32]. Significance was estimated by sample permutation. For gene sets without direction, absolute enrichment scores were used. As gene sets, we used the MSigDB Hallmark and Gene Ontology (GO) biological process sets [33]. For the GO terms, REVIGO [34] was used.

Single-cell reference profile construction and bulk cell deconvolution

We obtained the single-cell unnormalized read counts from 20,483 cells of 7 treatment-naive HGSOC patients [35]. Single-cell analysis was performed using Seurat [36]. Genes expressed in less than three cells were discarded from the further analysis. Cells were filtered to contain at least 1000 unique expressed genes and to have a percentage of mitochondrial transcripts of less than 50%, leaving 19,937 cells for further analysis. Cells were subsequently log normalised to 10,000 transcripts per cell. In addition, each cell was scored for G2/M and S cell cycle phases based on a gene list for the human genome [37]. Cell transcript counts were then corrected for the cell cycle phase scores, the number of unique molecular identifiers and the percentage of mitochondrial transcripts, by independently scaling and centring the residuals of a linear model for each listed variable.

Next, principal component analysis was performed on the 2000 most variable protein coding genes and the 20 first principal components were selected for clustering based on an elbow plot. Cluster resolution was set to 0.5, which yielded well defined clusters for further annotations. Uniform Manifold Approximation and Projections (UMAP) were constructed on the first 20 principal components to visualise the clustering.

To assist in annotating individual cell clusters, differentially expressed genes were calculated using Seurat for each individual cluster. The reference profiles were constructed from Seurat clusters by averaging the original transcriptome counts of all single cells belonging to the same Seurat cluster with subsequent normalisation to transcripts per million.

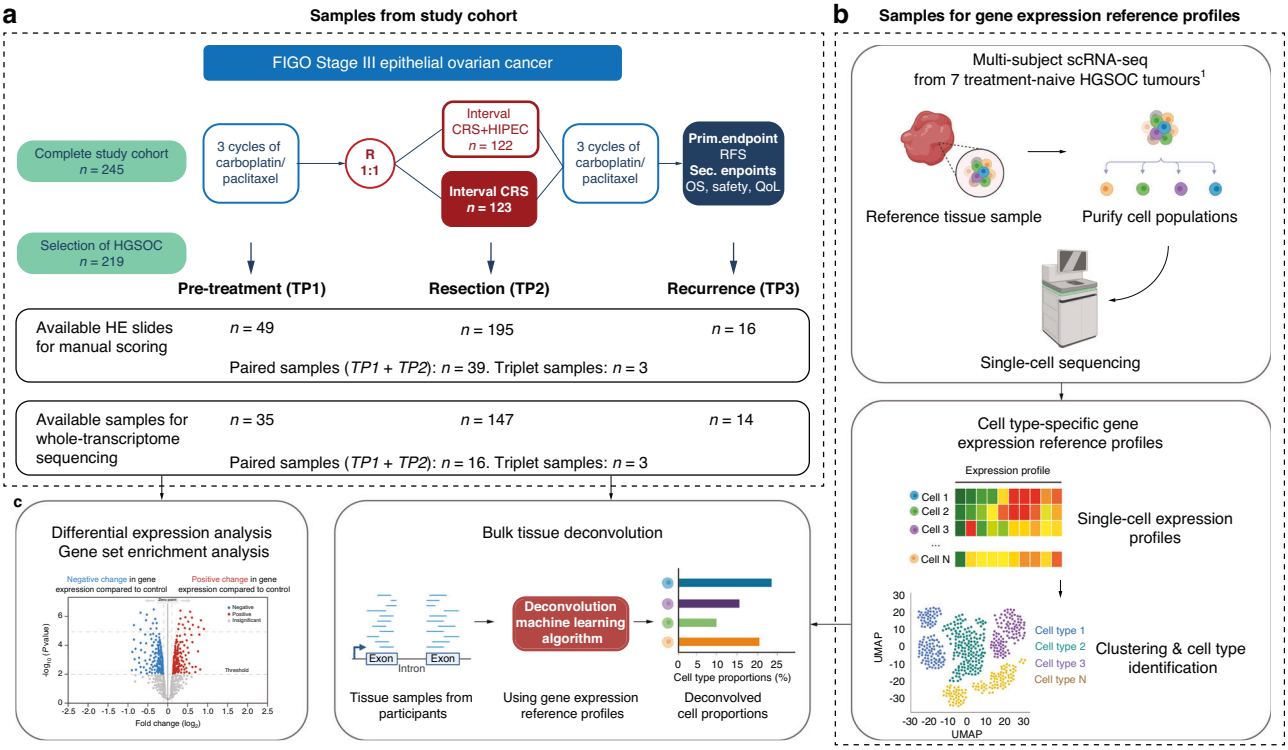

Fig. 2 Summary of methods diagram. a Samples from the OVHIPEC-1 study cohort were collected for HE-stained slides and whole-transcriptome sequencing at three time points: pre-treatment (TP1), surgical resection (TP2), and recurrence (TP3). Only patients with high-grade serous ovarian cancer were included in the analysis. **b** Cell-type-specific gene expression reference profiles were created using single-cell transcriptomic data from seven treatment-naïve high-grade serous ovarian cancer patients from a publicly available dataset (Olbrecht et al. [35]). Individual cells were isolated, RNA was extracted, and sequencing was performed. Clustering algorithms were then applied to group cells with similar gene expression profiles, and differentially expressed genes were calculated for each cluster. Clusters were annotated based on known marker genes or biological features, and reference profiles were constructed by averaging transcriptome counts within clusters. **c** A deconvolution algorithm, specifically Dampened Weighted Least Squares (DWLS), was employed to estimate the relative proportions of different cell types in samples obtained from the OVHIPEC-1 study cohort. This algorithm used the reference profiles derived from single-cell RNA sequencing to infer the cell-type fractions based on the gene expression signatures of the cells.

Dampened weighted least squares (DWLS) were used using default parameters to calculate the cell-type contributions per patient based on the cell-type reference profiles described in the previous section [16].

To validate the robustness of the deconvolution results, tumour slides of a subset of 75 patients were assessed by a board-certified pathologist (KKvdV) for immune cell percentage, as well as tumour cell percentage. Scoring was performed on tumours with consecutive H&E-stained tissue slides sourced from the same FFPE block used for bulk mRNA-seq, thereby minimising potential intra-patient heterogeneity between FFPE blocks.

Cell-type-based delta treatment score (DTS)

To investigate whether a set of features (cell types) is predictive of HIPEC benefit, we calculated a delta treatment score (DTS) [18]. DTS measures the relative risk of recurrence of a patient if treated with CRS over CRS-HIPEC based on a set of features and is calculated as follows. First, on the set of features to investigate (*CT*), which are a subset of the 24 cell types as predicted by the deconvolution, a multivariable Cox regression with pairwise treatment (*T*) interaction is fitted. Based on the CPH model a cell-type hazard score can be calculated for each patient in the test set under a given treatment. The cell type hazard score ($HS^{CT}_{p,T}$) for a set of features (*CT*) is calculated as follows:

$$HS^{CT}_{p,T} = \beta_1 * CT_p + \beta_2 * T + \beta_3 * CT_p * T \quad (1)$$

where, β_1 is the vector of coefficients for the main effects of features, *CT* is the vector of cell-type abundances in patient p, β_2 is the treatment effect, and β_3 is the vector of coefficients of the interaction between the features of patient p and the treatment. Finally, the DTS is calculated as follows:

$$DTS^{CT}_p = HS^{CT}_{p,T=1} - HS^{CT}_{p,T=0} \quad (2)$$

where, $HS^{CT}_{p,T=1}$ is the cell-type hazard score for patient p and features *CT* when treated with treatment $T = 1$ (CRS-HIPEC) and $HS^{CT}_{p,T=0}$ is the cell-type hazard score for patient p and features *CT* when treated with treatment $T = 0$ (CRS).

Determination of DTS cut-offs for the various risk groups

The predictive power of the DTS^{CT} was tested using a CPH model with treatment interaction. To avoid dataset-specific bias, DTS^{CT}_p scores for each feature set *CT* were calculated using leave-one-out validation, where a CPH model is fitted to all but one patient to calculate the DTS^{CT} for the remaining patient. A training and validation split was not possible in this study, as the training and validation sets would not allow for testing treatment interactions with sufficient statistical power. Furthermore, due to the randomised design of the study, important prognostic factors were evenly distributed between treatment arms (Supplementary Table 3). Therefore, clinical characteristics were not adjusted for in the analysis. For patient risk stratification, the median value was used as a cut-off to dichotomise the continuous DTS^{CT} into DTS^{CT}-high and DTS^{CT}-low, as no training set was available to select a cut-off in an unbiased way. Log-rank tests were used to test for significance in survival between risk groups.

RESULTS

The study included 219 patients diagnosed with high-grade serous ovarian carcinoma. Differential gene expression analysis and bulk RNA-seq deconvolution were performed using RNA-seq data from 35 pre-treatment samples, 147 resection samples, and 14 recurrence samples (Fig. 2). Histopathologic evaluation was

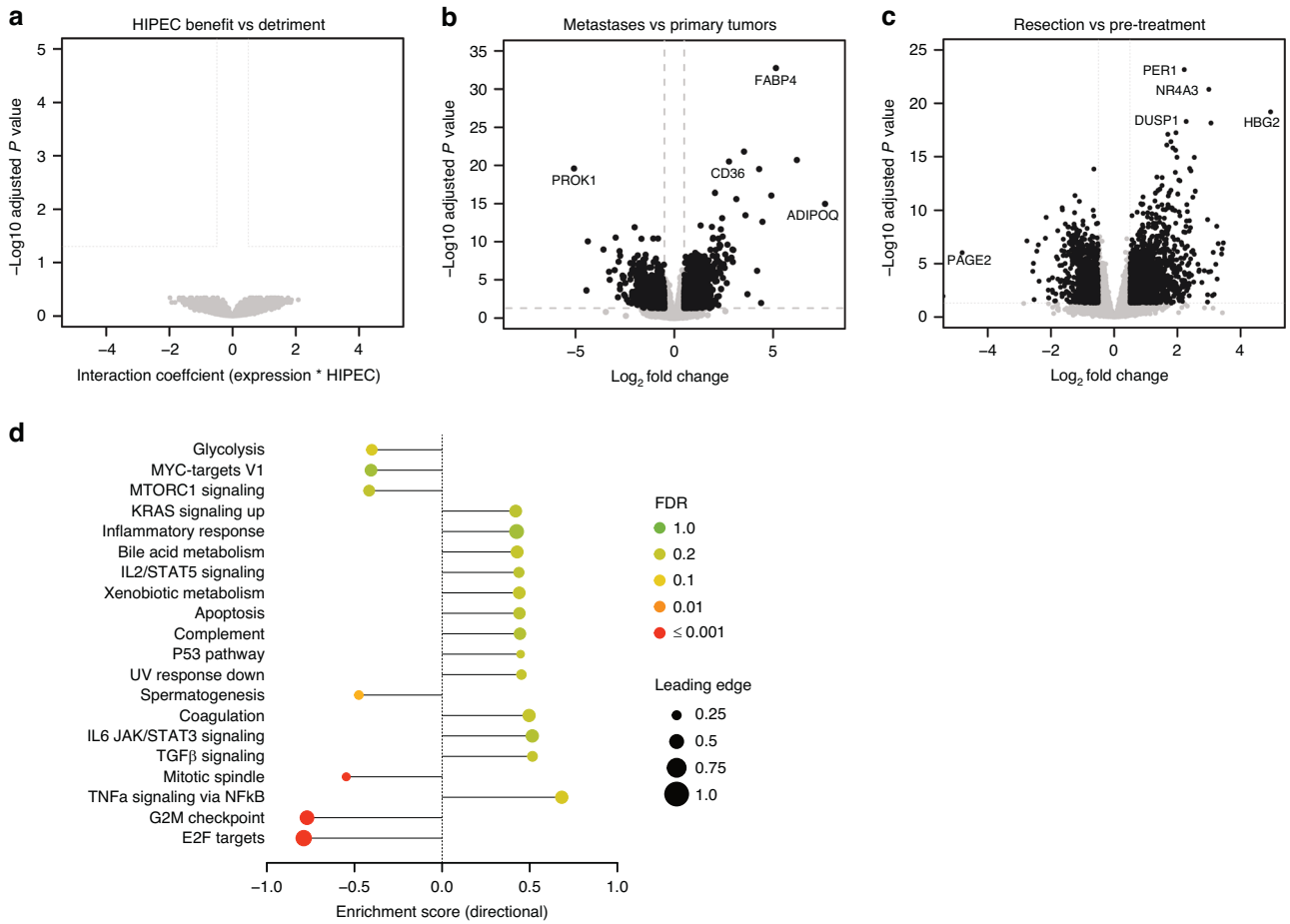

Fig. 3 Bulk differential gene expression analysis. a Volcano plot showing the interaction coefficients between each gene's expression level and HIPEC with survival in a Cox regression analysis, corrected for multiple hypothesis testing. No genes showed a significant association. **b** Volcano plot showing the difference of each gene's expression level between metastatic and primary tumour samples, among the resection samples. **c** Volcano plot showing the difference of each gene's expression level between pre-treatment samples and resection samples, with tissue location (primary vs metastatic) as covariate. **d** Gene set enrichment analysis for the comparison of resection samples to pre-treatment samples, given the MSigDB Hallmark gene sets. The graph shows the top 20 gene sets ordered by absolute enrichment score (bottom to top). The colour indicates the significance of the enrichment as a false discovery rate (FDR).

conducted on H&E-stained slides from FFPE blocks of 49 baseline samples, 195 resection samples, and 16 recurrence samples to validate the deconvolution results.

Differential expression analysis did not identify transcriptomic signatures associated with HIPEC benefit

We assessed whether bulk RNA-seq of the FFPE surgical resection samples (obtained following NACT) could define transcriptomic signatures associated with HIPEC benefit. We tested whether the interaction between the expression of each gene and treatment was associated with PFS in a CPH model. None of the genes had a significant association after correcting for multiple testing (Fig. 3a).

Although no significant associations were found with HIPEC benefits, we further explored differences between patients and samples and compared several subgroups in our dataset. First, we assessed differentially expressed genes between primary tumour samples and metastases (Fig. 3b). In metastases, we identified adipocyte-characteristic transcripts including *CD36, FABP4* and *ADIPOQ*.

Second, a comparison between pre-treatment and surgical resection samples showed profound differences. In total, 2906 genes were significantly different before and after NACT (Fig. 3c). Among these, DUSP1 is one of the most strongly upregulated genes after NACT and has previously been associated with chemotherapy resistance in HGSOC [38]. We used gene set enrichment analysis to identify specific sets of genes among the large number of differentially expressed genes (Fig. 3d). Here, gene sets associated with cell proliferation were significantly lower in the surgical resection samples, than in the pre-treatment samples. This is consistent with the killing of proliferative cancer cells by the NACT and indicates that the gene expression profiles contain biologically meaningful signals. Several signatures related to inflammation and stromal components, including TNFα and JAK/STAT signalling pathways, showed trends of increase after NACT. However, these differences did not reach significance, indicating the need for a different approach to find biomarkers predictive of HIPEC response.

Third, a comparison between the recurrence samples and the pre-treatment and resection samples revealed that gene sets associated with proliferation were significantly higher in the recurrence samples than in the resection samples (Supplementary Fig. 1A). However, there was no significant difference between the recurrence samples and the pre-treatment samples (Supplementary Fig. 1B). This is consistent with the outgrowth of cancer cells in the recurrence. Additionally, there were trends towards higher levels of inflammatory signalling pathways in the recurrence samples compared to the pre-treatment samples (Supplementary Fig. 1B). Although not statistically significant, this highlights the

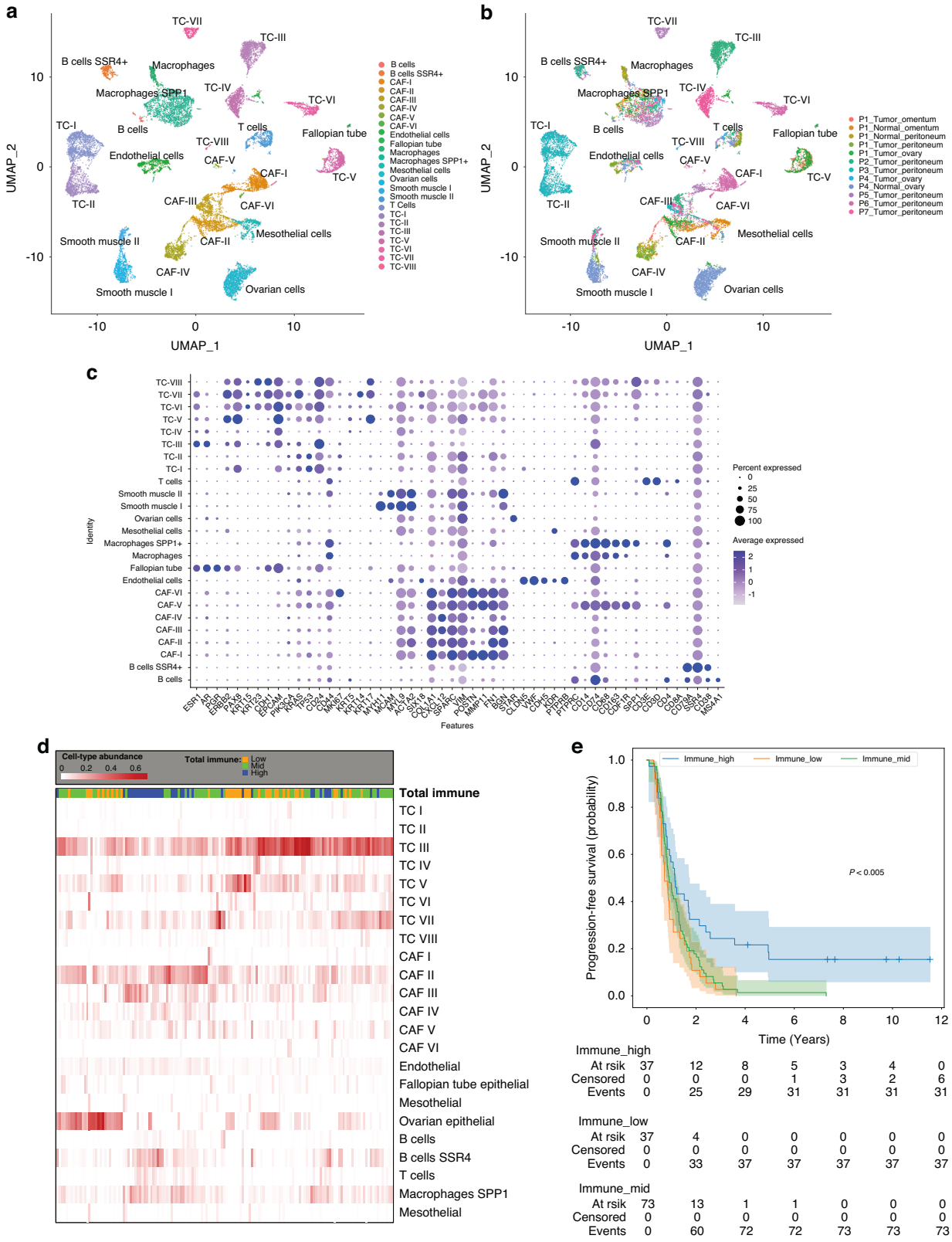

potential for further information to be uncovered through a deconvolution approach.

Despite the demonstrated associations in these subgroups, standard differential expression analysis yielded no significant associations with response to HIPEC.

Generation of independent reference profiles using single-cell mRNA sequencing of ovarian cancer

We subsequently aimed to deconvolve our bulk RNA-seq data to assess whether specific cell types, as well as their proportions, could predict a patient's benefit from HIPEC. Deconvolution

Fig. 4 Deconvolution of bulk RNA sequencing data to estimate cell-type abundance using single-cell expression reference profiles. **a** UMAP projection of single cells based on their normalised expression counts. Cells with similar expression profiles are proximally located, allowing for clustering, and annotating single cells according to their respective cell type. In total, Seurat-based clustering revealed 25 clusters, representing the expected cell types. **b** Annotation of the UMAP projection based on sample origin shows no patient overlap in TC clusters, while immune cell clusters consist of cells from multiple patients. **c** Expression of cell-type-specific marker genes within each cluster. Cell-type-specific markers are used to provide cell-type labels to individual Seurat-based clusters. **d** Heatmap showing cell-type abundances as estimated by single-cell deconvolution for every patient. Hierarchical clustering of patients shows a heterogeneous landscape of cell-type composition, with varying degrees of immune infiltration. **e** Kaplan–Meier Curve using quartile cut-offs (first 25% vs 25–75% vs 75% and beyond), shows a significant association of deconvolution-based immune cell abundance with PFS (two-sided log-rank *P* value = <0.005). CAF cancer-associated fibroblasts, TC tumour cells.

determines the proportions of different cell types in a bulk RNA-seq dataset using single-cell RNA-seq data as reference profiles. We used a publicly available single-cell dataset composed of 20,483 cells from 7 patients [35]. Seurat-based clustering revealed 25 clusters, representing the expected cell types (Fig. 4a). Clusters representing TME cells, such as B cells, T cells, and macrophages were composed of cells from multiple patients, whereas tumour cell (TC) clusters only contained cells from a single patient (Fig. 4b). We further delineated multiple clusters of cancer-associated fibroblasts (CAF), based on cell-type-specific marker genes. Some of these clusters had expression patterns that were unique to individual patients (Fig. 4c). Of note, no adipocyte cluster was identified reflecting the inefficient capture of this cell type in single-cell approaches, as previously described [39]. We then used this dataset for our deconvolution-based assessment of the bulk RNA-seq data.

Deconvolution of bulk mRNA data reveals robustly the cellular composition of tumours

Based on the 25 cell-type clusters we identified in HGSOC, we generated cell-type-specific reference profiles by averaging the gene expression within each cell-type cluster. These reference profiles were used for deconvolution to unravel the contribution of each cell type within the bulk mRNA-seq data of the 147 patients, with available sequencing data from the surgical resection sample (Fig. 4d), as well as from the pre-treatment and recurrence samples. Comparing the deconvolution-based cell-type fractions to the manual H&E-based cell-type scores, we observed good correlations between the two different cell-type estimations (Pearson correlation 0.73, Supplementary Fig. 2). Analysis of deconvolution-derived cell-type abundances from different time points reveals dynamic changes in cell populations over the course of disease progression and treatment response (Supplementary Figs. 3–5). Supplementary Fig. 6 shows the differences in cellular composition between primary and metastatic disease sites. Of note, paired samples from 16 patients from before and after NACT show a significant increase in macrophage abundance induced by NACT (Macrophages: $P = 0.02$; Macrophages SPP1: $P = 0.02$). While this increase can be observed in most paired samples, the extend of the observed changes in macrophage abundance following NACT is highly variable, with a subset of patients showing a decrease in macrophage abundance after NACT.

Distinct cellular compositions of high-grade serous ovarian tumours are associated with progression-free survival

Hierarchical clustering of the deconvolution-derived cell-type abundance matrix of the 147 samples from the resection time point, revealed pronounced heterogeneity in the cellular composition of HGSOC (Fig. 4d). We investigated whether different cellular compositions in HGSOC are associated with PFS. In our cohort, we identified as subset of patients with high immune cell abundance (i.e. sum of B cells, T cells, and macrophages). After adjusting for the addition or absence of HIPEC, the deconvolution-derived immune cell abundance (as a continuous variable) was significantly associated with PFS (HR 0.15, 0.03–0.62, *P* value = 0.01). Stratifying patients by their immune cell abundance revealed a subgroup with high immune cell abundance that had significantly prolonged PFS irrespective of treatment (Fig. 4e). Interestingly, the abundance of immune cells in the TME did not seem to correlate strongly with the abundance of other cell types such as CAFs or TCs (Supplementary Fig. 7).

Different tumour compositions are associated with HIPEC response

Next, we investigated whether the different deconvolution-derived cellular compositions allowed for the identification of a subset of patients with increased benefit from CRS over CRS-HIPEC, or vice versa. We modelled the differential treatment outcomes on PFS as the ratio of the hazards of a patient treated with CRS over CRS-HIPEC. The cell-type-based delta treatment score (DTS) score (see "Methods") delineates which treatment is more beneficial for a patient, where DTS < 0 indicates a benefit of the CRS-HIPEC treatment, and vice versa DTS > 0 indicates a better outcome without HIPEC. We investigated three different sets of cell-type (CT) abundances for their interaction with the treatment arm. We calculated a DTS^{CT} score for each set of cells belonging to TC, CAF and immune cells (IC) independently using leave-one-out cross-validation. The results indicated a significant interaction between DTS^{IC} and treatment in the CPH model for the set of immune cell abundances ($P_{interaction} < 0.005$). Conversely, the interactions for DTS^{TC} and DTS^{CAF} were not found to be significant ($P_{interaction} = 0.21$ and $P_{interaction} = 0.60$, respectively).

Subsequently, we dichotomised the continuous DTS^{IC} score into DTS^{IC}-high and DTS^{IC}-low using the median value as a cut-off. Survival analysis conducted on the resulting risk groups showed that patients with a low DTS^{IC} had a longer PFS when treated with CRS-HIPEC, whereas patients with a high DTS^{IC} had longer PFS in the absence of HIPEC (Fig. 5a, b). Analysis of the cell-type-specific contributions in calculating DTS^{IC} showed that both an increase in the abundance of B cells and the depletion of macrophages in the TME are associated with a lower DTS^{IC} (Fig. 5c). Cell-type abundances between DTS^{IC}-high and DTS^{IC}-low similarly show higher B-cell abundances and lower macrophage abundance in DTS^{IC}-low patients, while DTS^{IC}-high patients have overall lower B-cell abundance and a higher abundance of macrophages in the TME than DTS^{IC}-low patients (Fig. 5d, e). Furthermore, gene set enrichment analysis on the DTS^{IC} revealed upregulation of gene sets related to the interferon-alpha and interferon-gamma response pathways in patients with lower DTS^{IC} (Fig. 5f). This provides further validation for DTS^{IC}, as it shows correlation to the immune cell organisation of the sample even when going back to the bulk mRNA-seq data.

Histopathology of resection samples confirms macrophage absence or necrosis as predictors of enhanced HIPEC response

We performed the histopathological assessment of the HGSOC tissue samples from the primary tumour or the omentum resected during surgery (following NACT) in 102 CRS and 93 CRS-HIPEC patients (Fig. 1). An exploratory subgroup analysis suggested that within the subset of patients lacking macrophages, those who received HIPEC had more favourable OS compared to those who underwent surgery alone (HR 0.53 [95% CI 0.32–0.89]). In the subset of patients with macrophages present, overall survival was comparable between

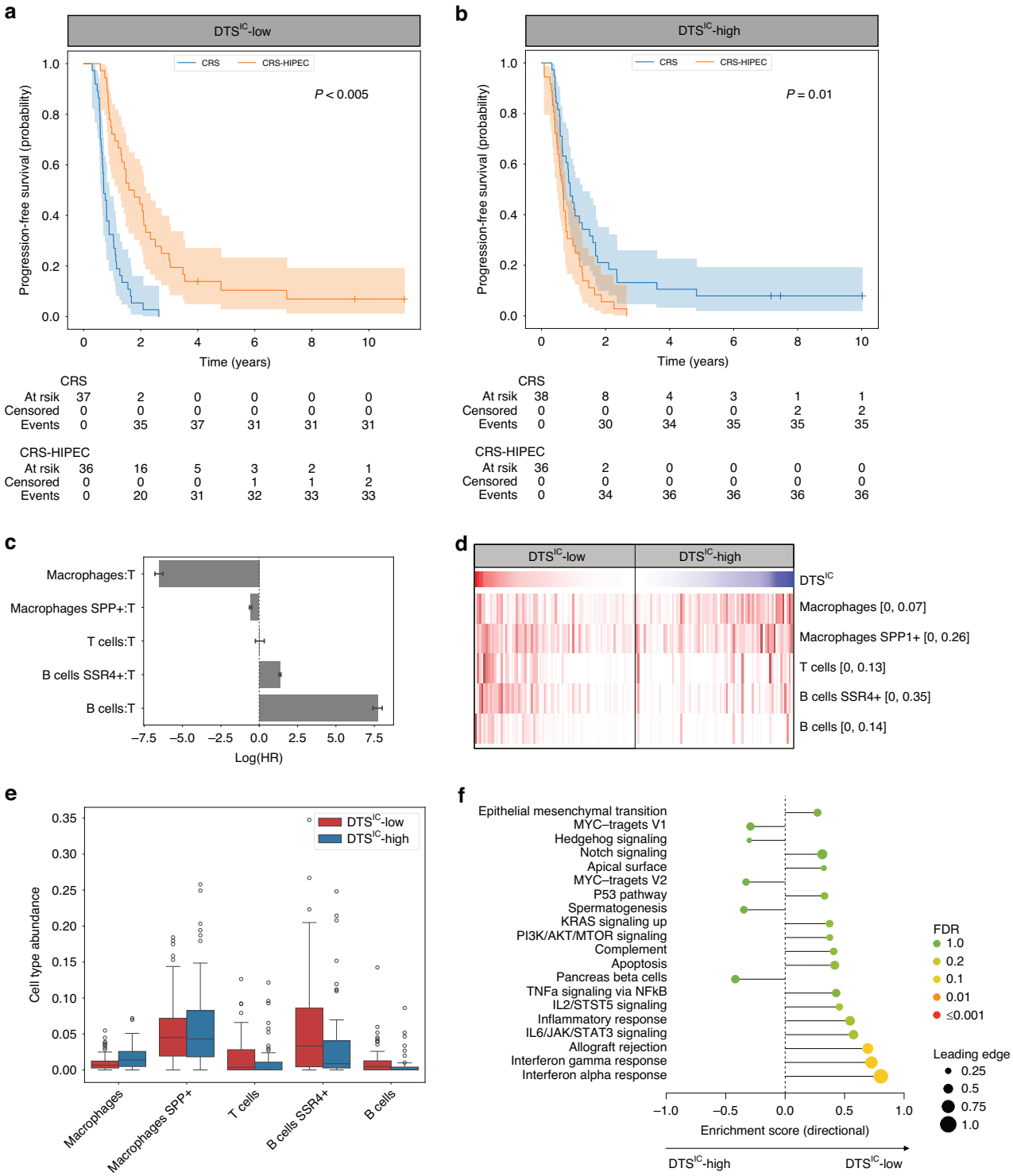

treatment arms. This suggests that there is a differential effect of treatment according to macrophage status ($P_{interaction} = 0.054$; Fig. 6). Stratification by other morphological variables did not reveal a differential treatment effect (Fig. 6). Exploratory subgroup analyses for PFS are shown in Supplementary Fig. 8.

DISCUSSION

In our study, we aimed to explore predictive biomarkers for HIPEC response to support tailored treatment to individual HGSOC patients. By applying deconvolution to bulk RNA-seq data, we found that this method robustly reveals the cellular composition of HGSOC from participants in the OVHIPEC-1 study. While standard differential gene expression analysis of bulk RNA-seq did not yield any discernible predictive biomarkers within our cohort, deconvolution methods demonstrated that HIPEC benefit may be predicted by the absence of macrophages and the presence of B cells in the TME. Manual pathologists scoring of morphologic features confirmed that macrophage absence was indicative of HIPEC response.

Fig. 5 Predictive delta treatment score based on single-cell deconvolution. Kaplan–Meier estimates for the (**a**) DTS^{IC}-low group and **b** DTS^{IC}-high group treated either with CRS or CRS-HIPEC. DTS^{IC} was dichotomised based on a median cut-off, where 50% of patients with the lowest DTS^{IC} were assigned to DTS^{IC}-low and 50% with the highest DTS^{IC} were assigned to DTS^{IC}-high. Patients in the DTS^{IC}-low group benefit significantly from HIPEC treatment ($P < 0.005$) over CRS, while in the DTS^{IC}-high group patients have significantly worse survival outcome when treated with HIPEC ($P = 0.01$). **c** Value of CPH interaction coefficients between treatment and cell-type features for DTS^{IC} averaged over all models in the leave-one-out validation. Error bars represent the 95% confidence intervals estimated by bootstrapping. A high positive interaction coefficient for a given cell type results in a lower DTS^{IC} and therefore better outcome for patients under HIPEC, while a high negative coefficient results in a higher DTS^{IC} and therefore better outcome under CRS, showing feature importance for DTS^{IC}. **d** Heatmap of cell-type abundances sorted according to DTS^{IC}. Given the prognostic significance of immune cells, both DTS^{IC}-low and DTS^{IC}-high patients show increased immune cell infiltration, while in DTS^{IC}-high patients, the TME contains a higher abundance of macrophages, contrasted by a higher B-cell abundance in DTS^{IC}-low patients. Cell-type abundances are normalised to the interval [0,1], with the interval of the unnormalized cell-type abundances with original feature value interval listed in brackets. **e** Absolute cell-type abundances for each immune cell cluster for DTS^{IC}-high and DTS^{IC}-low emphasising the absence of macrophages and the presence of B cells to be associated with differential HIPEC response. **f** Gene set enrichment analysis of the continuous deconvolution-derived DTS^{IC} shows upregulated immune-specific pathways in DTS^{IC}-low patients compared to DTS^{IC}-high patients. This finding provides further evidence supporting the validity of the deconvolution-derived DTS^{IC}, as the correlation between the patient-specific immune response and the differential HIPEC response remains even when reverting to the bulk mRNA-seq data. CRS cytoreductive surgery, DTS^{IC} immune cell delta treatment score, HIPEC hyperthermic intraperitoneal chemotherapy.

The absence of macrophages in the tumour microenvironment at surgical resection may be the effect of NACT or indicate an impaired anti-tumour immunity [40]. Host anti-tumour immune responses are associated with a significant improvement in overall survival in patients with HGSOC [12, 41]. For those patients lacking macrophages, HIPEC may be beneficial, given its potential to enhance the anti-tumour response through the immune-potentiating effects of the combination of hyperthermia and cisplatin [42]. Alternatively, patients without macrophages following NACT may be relatively resistant to systemic platinum-based chemotherapy, considering the known local immune activation induced by chemotherapy [43]. Local treatment of the peritoneum with high-dose heated chemotherapy might result in a higher sensitivity to HIPEC in contrast to those patients who are already relatively susceptible to systemic chemotherapy. This hypothesis is supported by the observed overlap of enriched pathways related to immune response in resection samples compared to pre-treatment samples (Fig. 3d) and in DTS^{IC}-low compared to DTS^{IC}-high samples (Fig. 5f), pointing to a potential link between the initial response to NACT and the subsequent response to HIPEC. This observation might also be consistent with the changes in macrophage abundances following NACT seen in paired samples (Supplementary Fig. 2). However, this requires additional investigation, since the number of paired samples is insufficient to draw significant conclusions. In addition, the state of tumour-associated macrophages (TAM) might contribute to our results. TAMs are an integral component of the TME in ovarian cancer and predominantly display a pro-tumour M2 phenotype [44]. M2-like TAMs limit the effector function of $CD8^+$ T cells in metastatic HGSOCs and are associated with poor overall survival [45, 46]. In this regard, the absence of immunosuppressive M2 macrophages in combination with the augmented local anti-tumour effect of the heated platinum may result in a better HIPEC response. However, in our experimental setup a discrimination between different TAM states (M1 or M2) was not possible.

Deconvolution further delineated a high abundance of B cells in the TME as a predictive biomarker for HIPEC treatment. Although the role of B cells in cancer is not yet fully understood, it might be hypothesised that heat shock proteins (HSP), released under hyperthermic conditions, modulate the immune response by affecting the activation and function of B cells [42, 47]. The favourable impact on survival following HIPEC aligns with the abundant presence of B cells at the tumour site. Further validation in other cohorts and mechanistic studies is required to assess macrophages and B cells in the TME as a predictive biomarker for HIPEC treatment. Moreover, validation in pre-treatment biopsies is needed to explore the feasibility of incorporating the biomarker into clinical practice, given that a biopsy after NACT deviates from standard of care.

Compared to the deconvolution of bulk RNA-seq data, our bulk gene expression analysis did not identify specific signatures associated with HIPEC benefit. This is in contrast to other studies [38] and might be explained by the fact that we accounted for gene selection bias and gene-gene correlations [48–50], and investigated a larger cohort of patients. When comparing differentially expressed genes between the primary tumour and metastatic sites, adipocyte-characteristic transcripts including *CD36, FABP4* and *ADIPOQ* were identified in metastases. These signatures likely result from omental fat tissue in metastatic samples, rather than representing inherent features of metastatic tumour cells. However, FABP4 was previously identified as a key determinant of metastatic potential of ovarian cancer [51, 52]. Moreover, the higher expression of *PROK1* in primary tumour samples may indicate residual normal ovarian tissue or might indicate true differences between metastatic and primary ovarian cancer cells. In line with this PROK1, endocrine gland-derived vascular endothelial growth factor has been linked to angiogenesis, proliferation and invasion in various malignant tumours [53]. When comparing pre-treatment samples with surgical resection samples, DUSP1 is strongly upregulated after treatment with NACT. This gene has previously been associated with chemotherapy resistance in HGSOC [38] and DUSP-inhibitors are being explored in mouse models of ovarian cancer [54]. Hence, our bulk gene expression analysis provided several relevant associations that may warrant follow-up study.

To our knowledge, this is the first study to use samples from a randomised controlled study to predict which ovarian cancer patients benefit most from HIPEC through transcriptomic profiling. Previous research in the same cohort showed that while *BRCA*-mutated tumours had better survival with CRS alone, no additional survival benefit was seen with HIPEC. Subgroup analysis revealed that HIPEC may be most beneficial for patients with homologous recombination-deficient (HRD) tumours lacking pathogenic *BRCA*1/2 mutations [2, 55]. These findings emphasise the importance of molecular profiling in personalising ovarian cancer treatment, highlighting the potential of identifying subgroups that may benefit more from HIPEC treatment. It should be noted that our evaluation excluded patients who achieved a complete pathological response to NACT, as no tumour tissue was available. Hence, our findings might not encompass the unique molecular characteristics of these exceptional complete responders. This could impact the generalisability of our results and introduce bias in our predictive models, although it is inherent to molecular research in clinical trials. Another limitation concerns the intra-patient heterogeneity commonly observed in ovarian tumours. The diverse cellular composition and molecular characteristics across different regions of a tumour can result in variations in treatment response and biomarker expression within a single

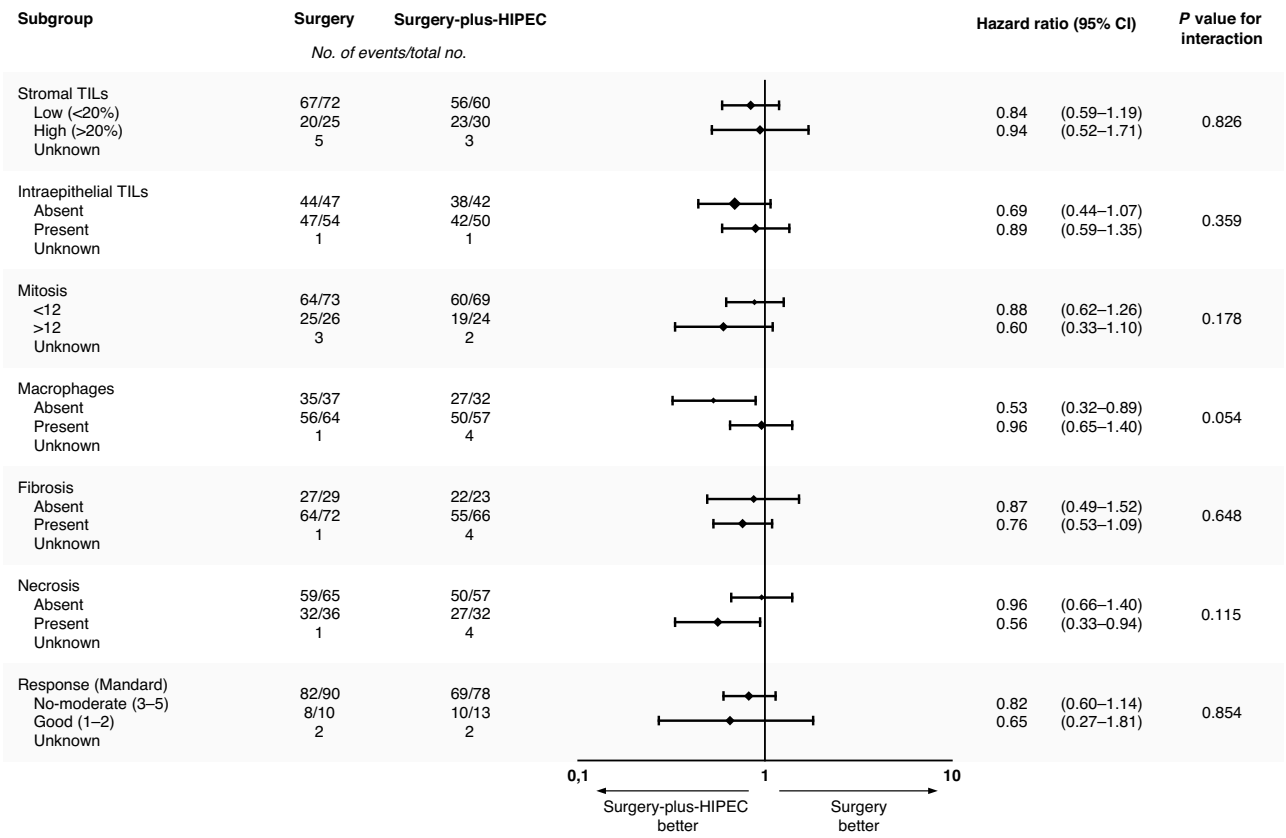

Fig. 6 Forest plot of exploratory subgroup analysis for overall survival based on histopathological assessment. Histopathological assessment was performed on tissue resected during interval CRS. We tested whether the interaction between the subgroup variable and treatment was associated with OS in a CPH model. The size of each diamond is proportional to the number of patients. TIL tumour infiltrating lymphocytes.

patient. Analysing only one tumour sample may not capture the full extent of this intra-patient heterogeneity and the substantial differences between various tumour sites. Nevertheless, this limitation is unavoidable, as it is difficult to justify multiple biopsies from each patient in a large cohort. With respect to inter-patient heterogeneity, the use of single-cell datasets with a limited number of patients for deconvolution might not comprehensively capture all TC and CAF cell types present in HGSOC. Although studies in breast cancer have shown no performance increase when using single-cell data from more than seven patients [18], further studies in HGSOC might benefit from a larger number of patients.

In summary, our study demonstrated that immune cell composition, in particular macrophages absence, may predict response to HIPEC in HGSOC. These hypothesis-generating findings need to be validated in future studies using cost-efficient and targeted methods such as immunohistochemistry, and may provide a potential opportunity for refined patient stratification to maximise treatment efficacy and avoid overtreatment.

DATA AVAILABILITY

Single-cell sequences for constructing reference profiles for deconvolution are publicly available [35], as well as count matrix and deconvolution results. The code used in generating the results is made available on https://github.com/cwlkr/DTSIC_HIPEC. Clinical data and RNA-seq data supporting this work are available upon reasonable request. Requests to access data should be made to the Netherlands Cancer Institute's scientific repository at repository@nki.nl, which will contact the corresponding author. The institutional review board of the Netherlands Cancer Institute will review all requests.

REFERENCES

1. van Driel WJ, Koole SN, Sikorska K, Schagen van Leeuwen JH, Schreuder HWR, Hermans RHM, et al. Hyperthermic intraperitoneal chemotherapy in ovarian cancer. New Engl J Med. 2018;378:230–40.
2. Aronson SL, Lopez-Yurda M, Koole SN, Schagen van Leeuwen JH, Schreuder HWR, Hermans RHM, et al. Cytoreductive surgery with or without hyperthermic intraperitoneal chemotherapy in patients with advanced ovarian cancer (OVHIPEC-1): final survival analysis of a randomised, controlled, phase 3 trial. Lancet Oncol. 2023;24:1109–18.
3. Auer RC, Sivajohanathan D, Biagi J, Conner J, Kennedy E, May T. Indications for hyperthermic intraperitoneal chemotherapy with cytoreductive surgery: a clinical practice guideline. Curr Oncol. 2020;27:146–54.
4. National Comprehensive Cancer Network. Ovarian Cancer (Version 3.2022) [Available from: https://www.nccn.org/login?ReturnURL=https://www.nccn.org/professionals/physician_gls/pdf/ovarian.pdf.
5. Chicago Consensus Working Group. The Chicago Consensus on peritoneal surface malignancies: management of ovarian neoplasms. Cancer. 2020;126:2553–60.
6. Lavoué V, Huchon C, Akladios C, Alfonsi P, Bakrin N, Ballester M, et al. [Part II drafted from the short text of the French guidelines entitled "Initial management of patients with epithelial ovarian cancer" developed by FRANCOGYN, CNGOF, SFOG, GINECO-ARCAGY and endorsed by INCa. (Systemic and intraperitoneal treatment, elderly, fertility preservation, follow-up)]. Gynecol Obstet Fertil Senol. 2019;47:111–9.
7. Lim MC, Chang SJ, Park B, Yoo HJ, Yoo CW, Nam BH, et al. Survival after hyperthermic intraperitoneal chemotherapy and primary or interval cytoreductive surgery in ovarian cancer: a randomized clinical trial. JAMA Surg. 2022;157:374–83.
8. Zhang AW, McPherson A, Milne K, Kroeger DR, Hamilton PT, Miranda A, et al. Interfaces of malignant and immunologic clonal dynamics in ovarian cancer. Cell. 2018;173:1755–69.e22.
9. Zhang Y, Tang H, Cai J, Zhang T, Guo J, Feng D, et al. Ovarian cancer-associated fibroblasts contribute to epithelial ovarian carcinoma metastasis by promoting angiogenesis, lymphangiogenesis and tumor cell invasion. Cancer Lett. 2011;303:47–55.

10. Dijkgraaf EM, Heusinkveld M, Tummers B, Vogelpoel LT, Goedemans R, Jha V, et al. Chemotherapy alters monocyte differentiation to favor generation of cancer-supporting M2 macrophages in the tumor microenvironment. Cancer Res. 2013;73:2480–92.
11. Sherman-Baust CA, Weeraratna AT, Rangel LB, Pizer ES, Cho KR, Schwartz DR, et al. Remodeling of the extracellular matrix through overexpression of collagen VI contributes to cisplatin resistance in ovarian cancer cells. Cancer Cell. 2003;3:377–86.
12. Hwang WT, Adams SF, Tahirovic E, Hagemann IS, Coukos G. Prognostic significance of tumor-infiltrating T cells in ovarian cancer: a meta-analysis. Gynecol Oncol. 2012;124:192–8.
13. Quail DF, Joyce JA. Microenvironmental regulation of tumor progression and metastasis. Nat Med. 2013;19:1423–37.
14. Thibault B, Castells M, Delord J-P, Couderc B. Ovarian cancer microenvironment: implications for cancer dissemination and chemoresistance acquisition. Cancer Metastasis Rev. 2014;33:17–39.
15. Newman AM, Liu CL, Green MR, Gentles AJ, Feng W, Xu Y, et al. Robust enumeration of cell subsets from tissue expression profiles. Nat Methods. 2015;12:453–7.
16. Tsoucas D, Dong R, Chen H, Zhu Q, Guo G, Yuan GC. Accurate estimation of cell-type composition from gene expression data. Nat Commun. 2019;10:2975.
17. Schelker M, Feau S, Du J, Ranu N, Klipp E, MacBeath G, et al. Estimation of immune cell content in tumour tissue using single-cell RNA-seq data. Nat Commun. 2017;8:2032.
18. Kester L, Seinstra D, van Rossum AGJ, Vennin C, Hoogstraat M, van der Velden D, et al. Differential survival and therapy benefit of patients with breast cancer are characterized by distinct epithelial and immune cell microenvironments. Clin Cancer Res. 2022;28:960–71.
19. Newman AM, Steen CB, Liu CL, Gentles AJ, Chaudhuri AA, Scherer F, et al. Determining cell type abundance and expression from bulk tissues with digital cytometry. Nat Biotechnol. 2019;37:773–82.
20. Chen B, Khodadoust MS, Liu CL, Newman AM, Alizadeh AA. Profiling tumor infiltrating immune cells with CIBERSORT. Methods Mol Biol. 2018;1711:243–59.
21. Zhang SC, Hu ZQ, Long JH, Zhu GM, Wang Y, Jia Y, et al. Clinical implications of tumor-infiltrating immune cells in breast cancer. J Cancer. 2019;10:6175–84.
22. Ali HR, Chlon L, Pharoah PD, Markowetz F, Caldas C. Patterns of immune infiltration in breast cancer and their clinical implications: a gene-expression-based retrospective study. PLoS Med. 2016;13:e1002194.
23. Ge P, Wang W, Li L, Zhang G, Gao Z, Tang Z, et al. Profiles of immune cell infiltration and immune-related genes in the tumor microenvironment of colorectal cancer. Biomed Pharmacother. 2019;118:109228.
24. Tamminga M, Hiltermann TJN, Schuuring E, Timens W, Fehrmann RS, Groen HJ. Immune microenvironment composition in non-small cell lung cancer and its association with survival. Clin Transl Immunol. 2020;9:e1142.
25. Moore K, Colombo N, Scambia G, Kim BG, Oaknin A, Friedlander M, et al. Maintenance olaparib in patients with newly diagnosed advanced ovarian cancer. New Engl J Med. 2018;379:2495–505.
26. Rustin GJ, Vergote I, Eisenhauer E, Pujade-Lauraine E, Quinn M, Thigpen T, et al. Definitions for response and progression in ovarian cancer clinical trials incorporating RECIST 1.1 and CA 125 agreed by the Gynecological Cancer Intergroup (GCIG). Int J Gynecol Cancer. 2011;21:419–23.
27. Mandard AM, Dalibard F, Mandard JC, Marnay J, Henry-Amar M, Petiot JF, et al. Pathologic assessment of tumor regression after preoperative chemoradiotherapy of esophageal carcinoma. Clinicopathologic correlations. Cancer. 1994;73:2680–6.
28. Li B, Dewey CN. RSEM: accurate transcript quantification from RNA-Seq data with or without a reference genome. BMC Bioinforma. 2011;12:323.
29. Dobin A, Davis CA, Schlesinger F, Drenkow J, Zaleski C, Jha S, et al. STAR: ultrafast universal RNA-seq aligner. Bioinformatics. 2013;29:15–21.
30. Love MI, Huber W, Anders S. Moderated estimation of fold change and dispersion for RNA-seq data with DESeq2. Genome Biol. 2014;15:550.
31. Bismeijer T, Kim Y. FlexGSEA: flexible gene set enrichment analysis (Version v1.3). Zenodo 2019. https://doi.org/10.5281/zenodo.2616660.
32. Subramanian A, Tamayo P, Mootha VK, Mukherjee S, Ebert BL, Gillette MA, et al. Gene set enrichment analysis: a knowledge-based approach for interpreting genome-wide expression profiles. Proc Natl Acad Sci USA. 2005;102:15545–50.
33. Liberzon A, Birger C, Thorvaldsdóttir H, Ghandi M, Mesirov JP, Tamayo P. The Molecular Signatures Database (MSigDB) hallmark gene set collection. Cell Syst. 2015;1:417–25.
34. Supek F, Bošnjak M, Škunca N, Šmuc T. REVIGO summarizes and visualizes long lists of gene ontology terms. PLoS ONE. 2011;6:e21800.
35. Olbrecht S, Busschaert P, Qian J, Vanderstichele A, Loverix L, Van Gorp T, et al. High-grade serous tubo-ovarian cancer refined with single-cell RNA sequencing: specific cell subtypes influence survival and determine molecular subtype classification. Genome Med. 2021;13:111.
36. Hao Y, Hao S, Andersen-Nissen E, Mauck WM 3rd, Zheng S, Butler A, et al. Integrated analysis of multimodal single-cell data. Cell 2021;184:3573–87.e29.
37. Oza AM, Castonguay V, Tsoref D, Diaz-Padilla I, Karakasis K, Mackay H, et al. Progression-free survival in advanced ovarian cancer: a Canadian review and expert panel perspective. Curr Oncol. 2011;18:S20–7.
38. Kang Y, Nagaraja AS, Armaiz-Pena GN, Dorniak PL, Hu W, Rupaimoole R, et al. Adrenergic stimulation of DUSP1 impairs chemotherapy response in ovarian cancer. Clin Cancer Res. 2016;22:1713–24.
39. Emont MP, Jacobs C, Essene AL, Pant D, Tenen D, Colleluori G, et al. A single-cell atlas of human and mouse white adipose tissue. Nature. 2022;603:926–33.
40. Heath O, Berlato C, Maniati E, Lakhani A, Pegrum C, Kotantaki P, et al. Chemotherapy induces tumor-associated macrophages that aid adaptive immune responses in ovarian cancer. Cancer Immunol Res. 2021;9:665–81.
41. Montfort A, Barker-Clarke RJ, Piskorz AM, Supernat A, Moore L, Al-Khalidi S, et al. Combining measures of immune infiltration shows additive effect on survival prediction in high-grade serous ovarian carcinoma. Br J Cancer. 2020;122:1803–10.
42. Huffman OG, Chau DB, Dinicu AI, DeBernardo R, Reizes O. Mechanistic insights on hyperthermic intraperitoneal chemotherapy in ovarian cancer. Cancers. 2023;15:1402.
43. Jiménez-Sánchez A, Cybulska P, Mager KL, Koplev S, Cast O, Couturier D-L, et al. Unraveling tumor–immune heterogeneity in advanced ovarian cancer uncovers immunogenic effect of chemotherapy. Nat Genet. 2020;52:582–93.
44. Schweer D, McAtee A, Neupane K, Richards C, Ueland F, Kolesar J. Tumor-associated macrophages and ovarian cancer: implications for therapy. Cancers. 2022;14:2220.
45. Hensler M, Kasikova L, Fiser K, Rakova J, Skapa P, Laco J, et al. M2-like macrophages dictate clinically relevant immunosuppression in metastatic ovarian cancer. J Immunother Cancer. 2020;8:e000979.
46. Zhang M, He Y, Sun X, Li Q, Wang W, Zhao A, et al. A high M1/M2 ratio of tumor-associated macrophages is associated with extended survival in ovarian cancer patients. J Ovarian Res. 2014;7:19.
47. Cohen-Sfady M, Nussbaum G, Pevsner-Fischer M, Mor F, Carmi P, Zanin-Zhorov A, et al. Heat shock protein 60 activates B cells via the TLR4-MyD88 pathway. J Immunol. 2005;175:3594–602.
48. Maleki F, Ovens K, Hogan DJ, Kusalik AJ. Gene set analysis: challenges, opportunities, and future research. Front Genet. 2020;11:654.
49. Ambroise C, McLachlan GJ. Selection bias in gene extraction on the basis of microarray gene-expression data. Proc Natl Acad Sci USA. 2002;99:6562–6.
50. Goeman JJ, Bühlmann P. Analyzing gene expression data in terms of gene sets: methodological issues. Bioinformatics. 2007;23:980–7.
51. Gharpure KM, Pradeep S, Sans M, Rupaimoole R, Ivan C, Wu SY, et al. FABP4 as a key determinant of metastatic potential of ovarian cancer. Nat Commun. 2018;9:2923.
52. Nieman KM, Kenny HA, Penicka CV, Ladanyi A, Buell-Gutbrod R, Zillhardt MR, et al. Adipocytes promote ovarian cancer metastasis and provide energy for rapid tumor growth. Nat Med. 2011;17:1498–503.
53. Corlan AS, Cîmpean AM, Jitariu AA, Melnic E, Raica M. Endocrine gland-derived vascular endothelial growth factor/prokineticin-1 in cancer development and tumor angiogenesis. Int J Endocrinol. 2017;2017:3232905.
54. Sanders BE, Yamamoto TM, McMellen A, Woodruff ER, Berning A, Post MD, et al. Targeting DUSP activity as a treatment for high-grade serous ovarian carcinoma. Mol Cancer Ther. 2022;21:1285–95.
55. Koole SN, Schouten PC, Hauke J, Kluin RJC, Nederlof P, Richters LK, et al. Effect of HIPEC according to HRD/BRCAwt genomic profile in stage III ovarian cancer—results from the phase III OVHIPEC trial. Int J Cancer. 2022;151:1394–404.

ACKNOWLEDGEMENTS

The authors thank all patients and their families and caregivers for participating in the present study. We thank the Core Facility of Molecular Pathology and Biobanking, S Cornelissen and D Peters for their support in processing of the samples; RJC Kluin, W Brugman, and the Genomics Core Facility for their support with sequencing; the principal investigators of the participating sites in patient recruitment and sample acquisition. The present study was funded by the Dutch National Cancer Foundation (KWF) and sponsored by the NKI. The funding sources had no role in the design and execution of the study, data analysis or writing of the manuscript.

AUTHOR CONTRIBUTIONS

KH, LvK, JvR, SR, WJvD, GSS, SNK and CARL were involved in the conceptualisation. WJvD was the coordinating principal investigator for the clinical study and was responsible for funding acquisition. SR, JvR and GSS were also responsible for funding acquisition. SLA, SNK, GSS and WJvD were involved in clinical data collection. KKvdV,

JS and HMH performed manual pathology scoring. MA performed the processing of the tissue samples. SLA performed the histopathological analysis under the supervision of MLY. CW performed the deconvolution analyses under the supervision of LvK, KH and SR. BT performed the gene expression analyses. SLA, CW, BT, KH and LvK, interpreted the data. SLA, CW, BT and KH wrote the original draft of the manuscript. KH, LvK, JvR, SR, WJvD and GSS supervised the study. All authors were involved in critically revising the report. All authors approved the final version and took responsibility for the decision to submit the manuscript for publication.

FUNDING

The OVHIPEC-1 trial was funded by the Dutch Cancer Foundation (KWF Kankerbestrijding; NKI 2006–4176, to WJvD). Further financial support came from the Department of Defense Ovarian Cancer Research Program (Award No. W81XWH-22-1-0557), the Swiss National Science Foundation (320030M_219453), the Swiss Cancer League (KFS-5519-02-2022), and the ISREC Foundation (to SR). JvR received funding from the Josef Steiner Cancer Research Foundation.

COMPETING INTERESTS

KKVdV has served on advisory boards for Exact Sciences and AstraZeneca. HMH received honoraria from Roche Diagnostics BV. GSS has received institutional research support from Merck Sharp & Dohme, Agendia, AstraZeneca, Roche, and Novartis, and consulting fees from Biovica and Seagen. KH is a former employee at the Netherlands Cancer Institute and is currently working for Roche, Pharmaceutical Sciences, Basel, Switzerland. The research for this project was conducted in her position of researcher at the NKI. The remaining authors declare no competing interests.

ETHICS APPROVAL AND CONSENT TO PARTICIPATE

The protocol was approved by the local ethics committee at each of the participating centres. All patients provided written informed consent prior to enrolment. This study was performed in accordance with the Declaration of Helsinki.

CONSENT FOR PUBLICATION

Not applicable.

ADDITIONAL INFORMATION

Supplementary information The online version contains supplementary material available at https://doi.org/10.1038/s41416-024-02731-6.

Correspondence and requests for materials should be addressed to Willemien J. van Driel.

OVHIPEC-1 STUDY GROUP

W. J. van Driel[1], H. M. Hermans[14], J. H. Schagen van Leeuwen[15], H. W. R. Schreuder[16], M. D. J. M. van Gent[17], M. A. P. C. van Ham[18], H. J. G. Arts[19], P. A. van Dam[20] and P. Vuylsteke[21]

[14]Department of Gynecology and Obstetrics, Catharina Hospital, Eindhoven, The Netherlands. [15]Department of Obstetrics & Gynecology, Sint Antonius Hospital, Nieuwegein, The Netherlands. [16]Department of Gynecologic Oncology, UMC Utrecht Cancer Center, Utrecht, The Netherlands. [17]Center for Gynecologic Oncology Amsterdam, Department of Obstetrics and Gynecology, Amsterdam University Medical Center, Amsterdam, The Netherlands. [18]Department of Gynecologic Oncology, Radboud University Medical Centre, Nijmegen, The Netherlands. [19]Department of Gynecologic Oncology, University Medical Center Groningen, Groningen, The Netherlands. [20]Department of Gynecologic Oncology, University Hospital Antwerp, Antwerp, Belgium. [21]Department of Medical Oncology, UCL Louvain, CHU Namur Sainte-Elisabeth, Namur, Belgium.

A full list of members and their affiliations appears in the Supplementary Information.